ARTICLE

Gold Cluster Formation with Phosphine Ligands: Etching as a Size-Selective Synthetic Pathway for Small Clusters?

John M. Pettibone and Jeffrey W. Hudgens*

Chemical and Biochemical Reference Data Division, National Institute of Standards and Technology, Gaithersburg, Maryland 20899, United States

ABSTRACT Triphenylphosphine (PPh_3) is commonly used during syntheses of stable, closed-shell monolayer protected clusters (MPCs). Models of transition metal (TM) cluster and nanoparticle syntheses commonly assign PPh_3 a passive role as a chemical placeholder, electron balancing species, or surfactant. This study provides the first direct evidence that PPh_3 is a proactive etching agent that promotes the formation of specific closed-shell cluster sizes. To observe this effect, we developed a colorimetric tool that simultaneously monitors size distribution and population of PPh_3-protected clusters as a function of time. The distribution of the clusters is assigned to different bin sizes by chemical conversion with L^3 (L^3 = 1,3-bis(diphenylphosphino)propane): (i) total conversion of PPh_3-protected Au_8 and Au_9 clusters into $[Au_6L^3{}_4]^{2+}$ and (ii) ligand exchange with $[Au_x(PPh_3)_y]^{z+}$ ($10 \leq x \leq 13$) clusters to form L^3-protected Au_{10} and Au_{11} clusters. Evolution of the nascent cluster distribution in ethanol and methanol solvent systems was monitored by the colorimetric assay, which revealed a cyclic process of growth and etching reactions around the most stable cluster species to form nearly monodisperse product distributions. We formally define the population growth of specific clusters through cyclic processing of the Au MPCs as "size selective" processing. The current study highlights the need for incorporating bidirectional processing, including relative rate information, into TM kinetic models for ligands with growth and etching efficacy.

KEYWORDS: colorimetric assay · growth mechanism · nucleation · ligand-protected clusters · nanoparticles · triphenylphosphine

The development of synthetic techniques for monolayer protected clusters (MPCs) continues to be the topic of ongoing research because MPCs exhibit unique nuclearity-selective properties that differ from their bulk metal counterparts. In general, relatively monodisperse MPC syntheses have been developed with protecting ligands such as thiols, amines, and polymeric ligands, which have multiple roles as stabilizers, place holders, or etching agents.[1−7] Understanding the specific role of the ligands is necessary for maximizing their potential for material development. Phosphine-protected Au nanoclusters have been examined for catalysis, imaging, drug delivery platforms, and targeting agents.[8−11] These MPCs can also be building blocks for larger, higher order structures. The protecting ligands impact the physicochemical properties of the monolayer protected clusters including solubility, reactivity, optical properties, and aggregation. Triphenylphosphine (PPh_3) and other phosphorus ligands are currently described as place holders or surfactants in cluster formation because they can be readily replaced through ligand exchange reactions;[7,12−14] however, previous synthetic approaches that form specific MPCs or ligated nanoparticles of different sizes describe PPh_3 as a useful protecting ligand for selectivity,[15−21] suggesting that PPh_3 can play substantial roles during cluster formation.

Syntheses of solution-phase, phosphine-protected gold clusters commonly involve the reduction of an oxidized Au precursor in the presence of PPh_3, resulting in a distribution of nascent clusters. To narrow the product distribution, synthesis procedures may include the adjustment of synthetic parameters controlling specific reaction rates, for example, reduction, through changes in stir rate, temperature, reducing agent, *etc.* Additional separation steps may be needed to isolate desired products, increasing the overall time and cost of MPC syntheses. The reduction kinetics of oxidized Au precursors are partially controlled by the reaction between the primary reducing reagent and solvent (or solvent mixture), and these reaction rates have been shown to strongly affect cluster size.[22−24] For example, substitution of methanol for acetone during the synthesis of thiol-protected Au_{38} clusters was demonstrated to increase the nuclearity of nascent clusters; however, the governing mechanism was not discussed.[25] Different alcohols have reportedly different reaction rates with $NaBH_4$,[22,24,26] which can also directly affect the nascent cluster formation.[27] The reduction of $AuClPPh_3$ by $NaBH_4$ in methanol systems is relatively

* Address correspondence to hudgens@nist.gov.

Received for review January 5, 2011 and accepted March 7, 2011.

Published online March 07, 2011
10.1021/nn200053b

rapid and initially produces a large distribution of ligated cluster nuclearities,[2] but some tendency to form specific cluster sizes has been observed in the presence of phosphine ligands.

More recently, diphosphine ligands have shown a propensity to form narrow (monodisperse) distributions of phosphine-protected gold MPCs, indicating a more influential role in the formation mechanism for phosphorus-containing ligands in fast reducing environments,[1,2,28] and we have developed synthetic techniques for producing tunable, monodisperse clusters.[28] The propensity to form specific MPCs in relatively fast reducing environments would imply the presence of a correction step involving phosphine ligands, which is similar to product formation with thiols, amines, and other polymers, but there have been no direct measurements of phosphine etching efficacy. The size-selectivity of such synthetic processes is not well understood. Although significant work has been conducted on synthesizing phosphine protected clusters, the formation mechanism is not well characterized, particularly regarding the specific role of the PPh_3 as protecting ligands during reduction, cluster core formation, and subsequent MPC growth, which hinders the development of more accurate models.

Current models for the reduction of ligand-transition metal (TM) complexes in solution apply unidirectional product formation exclusively through growth. Such models do not account for size-specific product formation in fast reducing environments, where a relatively large distribution of nascent, stable clusters is formed. The development of accurate models will result from identification of specific reaction pathways driving product formation. Reaction pathways could be identified if direct measurements of different Au MPCs were able to be monitored with information regarding size distribution and population density as a function of time. The evolution of the cluster distribution would aid in identifying reactions occurring in the solution and especially competing growth and correcting (etching) reactions. Currently, no experimental methods are available for simultaneously monitoring the distribution and population density of TM clusters as a function of time, and instruments such as dynamic light scattering (DLS) have limited abilities to measure MPC distributions accurately. Reduction and subsequent nucleation reactions forming neutral species cannot be easily monitored by mass spectrometry, and other optical measurements of MPC distributions cannot distinguish effectively the primary clusters present; therefore, a new monitoring tool is needed to simultaneously probe the distribution and population density of products as a function of time.

This study identifies a dual role for PPh_3 as a protecting and proactive etching agent during ligated Au cluster formation. Monodisperse products are formed in the synthesis resulting from a competing cyclic process of growth and etching steps around stable, closed-shell ligated-TM clusters and not due solely to degradation pathways. The stable, closed-shell ligated-TM clusters resist etching and this promotes accumulation and/or growth. We formally define the competing reactions as "size-selective processing". The application of the size-selective methodology requires only some knowledge of the relative rates of cycling around the more stable products, allowing multiple products to be selectively synthesized. To monitor processing and to measure relative reaction rates, we develop a colorimetric assay that measures the relative $[Au_x(PPh_3)_y]^{z+}$ (including $z = 0$) populations of the core nuclearity sets, $\{Au_8, Au_9\}$ and $\{Au_x: x \geq 10\}$. We use the colorimetric assay to obtain the first direct evidence that PPh_3 has a dual role as a protective and proactive etching agent. PPh_3 is a relatively weak binding phosphorus ligand and is a useful model ligand to extrapolate to other systems involving stronger binding diphosphine ligands. The current study also provides important experimental evidence necessary for the development of better models describing the formation of monodisperse, ligand-protected clusters from ligand:metal complexes, which utilize ligands with inherent protecting and etching efficacy.

RESULTS AND DISCUSSION

In the following sections we characterize synthesis solutions with ultraviolet−visible (UV−vis) spectroscopy, dynamic light scattering (DLS), and electrospray ionization mass spectrometry (ESI-MS). We compare the collection of this data with data obtained from a newly developed colorimetric assay that enables us to assess temporally the relative distributions and population densities between two size bins of ligand-capped gold clusters. The sets are defined by $\{Au_8, Au_9\}$ and $\{Au_x: x \geq 10\}$. We devise this technique on the basis of known reactions for PPh_3, L^3, and $[Au_x(PPh_3)_y]^{z+}$. The characterization of the solutions allows for the elucidation of specific reaction pathways for size-selective properties of PPh_3, which should prove ubiquitous in other size-selective TM systems. The incorporation of the phosphine ligand properties into current TM models is also discussed.

Optical and Mass Spectrometry Characterization of $AuClPPh_3$ Reduction by $NaBH_4$. We have used UV−vis, ESI-MS, and DLS measurements to follow the $[Au_xPPh_3)_y]^{z+}$ products obtained from the reduction of $AuClPPh_3$ by $NaBH_4$ in both methanol and ethanol solvent systems. Figure 1 shows a sequence of UV−vis spectra observed in 1:1 methanol/chloroform solution for reaction times (t_{react}) between $t_{react} = 1$ h to $t_{react} = 142$ h, where $t_{react} = 0$ is the time point where $NaBH_4$ is added to the synthesis solution. At early time points ($t_{react} = 0$ h to $t_{react} = 48$ h) UV−vis spectra exhibit a faint shoulder, centered between 450 and 500 nm, that is consistent with previous studies of MPCs with reported diameters >1 nm.[29,30] With increasing time, the spectra develop more distinct features between 400 and 500 nm, which correspond to $[Au_x(PPh_3)_y]^{z+}$ clusters with gold atom nuclearity, $x \leq 13$.[31,32] Solution phase species exhibit absorption bands of $\lambda_{max} \approx 415$ nm and $\lambda_{max} \approx 470$ nm, which are consistent with previously reported PPh_3-capped Au_8 species.[32] ESI-MS data from this solution (not shown) exhibit ion peaks from $[Au_8(PPh_3)_7]^{2+}$ clusters only. From the work of Hudgens, *et al.*, we allow that a substantial fraction of the initial clusters may form with neutral charge, which would render them inaccessible to ESI-MS analyses.[31] The sensitivity of UV−vis spectroscopy would remain undiminished for detecting neutral, PPh_3-ligated Au_9 clusters.

For a synthesis repeated in 1:1 methanol/diethyl ether,[33] Figure 2 shows the UV−vis spectrum and DLS data observed at selected times. Again, UV−vis spectra obtained at early times (*e.g.*, t_{react} = 0.5 h) are featureless (Figure 2A, trace b); however, by t_{react} = 48 h, distinct Au MPCs with core nuclearity $x \leq 13$ are evidenced by the strong absorption at 440 nm (Figure 2A, trace b), which is a band characteristic of ligated Au_9 clusters.[32] In contrast, the ESI-MS of this solution (not shown) displays predominantly a $[Au_8(PPh_3)_7]^{2+}$ peak, as observed in the 1:1 methanol/chloroform solution. ESI-MS peaks correlating to the presence of $[Au_9(PPh_3)_8]^{3+}$ or $[Au_9(PPh_3)_8]^{+}$ are not observed. $[Au_9(PPh_3)_8]^{+}$ is expected to appear near 3871 *m/z*, which is at the upper limit for ion transmission through the quadrupole and ESI source; therefore, its absence may reflect transmission limitations of the instrument. Alternately, the absence of these ligated Au_9 species may indicate that they are neutral clusters.

The cluster size distributions in diethyl ether solution samples are monitored with DLS as a function of time (Figure 2B). Initially ($t_{react} \approx$ 10 min), several distinct hydrodynamic diameters (D_h) of Au species are observed ranging from $D_h \approx 1$ nm to ~4800 nm. Over the next 24 h, the distribution of clusters changes from a large distribution of colloids to a relatively narrower distribution centered near $D_h \approx 200$ nm. At t_{react} = 48 h, when UV−vis spectra indicate that the solution contains PPh_3-protected Au_9 clusters, the DLS measurements indicate that the mean diameter of gold colloids has decreased in size. With increasing time the DLS measurements indicate that the measured colloid size steadily decreases, and at t_{react} = 62 h the colloids have measured hydrodynamic diameters near $D_h \approx 40$ nm. The putative narrowing dispersity of the colloids over time observed in the UV−vis measurements occurs concomitantly with the decreasing colloid size measured in DLS. However, the distribution and population density of specific cluster sizes cannot be determined with confidence. The diameters reported in the DLS measurements represent the colloids present in the solution, and identification of the primary cluster sizes is intractable. Notably, the sensitivity

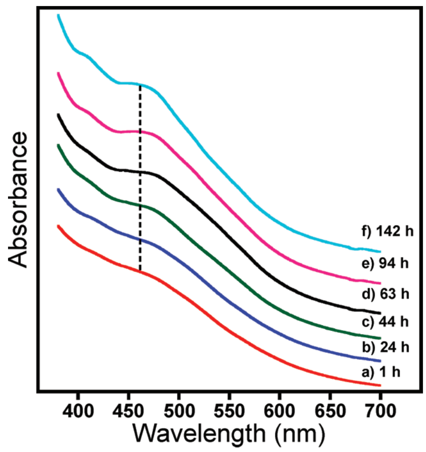

Figure 1. UV−vis measurements of $AuClPPh_3$ reduction with $NaBH_4$ as function of time in methanol/chloroform solutions from t_{react} = 1−142 h. The shoulder centered near 460 nm becomes more pronounced with increasing time.

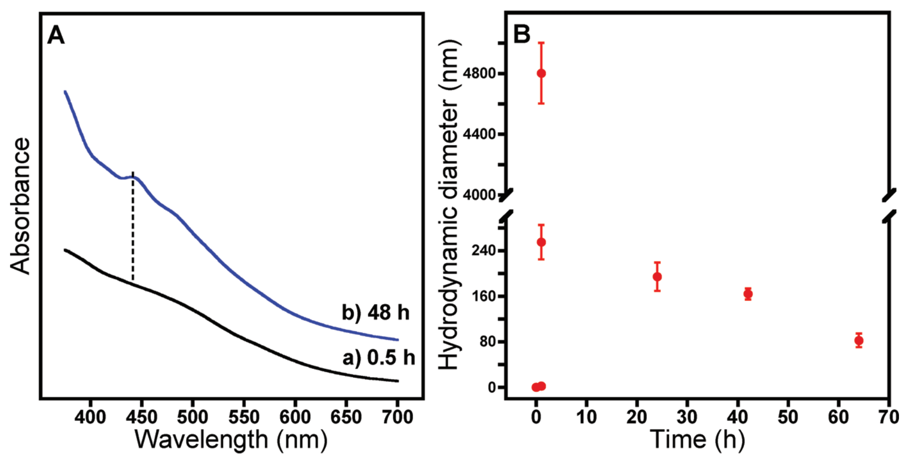

Figure 2. The Au clusters measured by UV−vis (A) and DLS (B) in 1:1 methanol/diethyl ether mixture at t_{react} = 0.5 h and t_{react} = 48 h. The growth of the 440 nm absorption band correlates to the formation of Au_9 clusters. The DLS data show a shift from larger to smaller colloids present in solution between t_{react} = 10 min and t_{react} = 62 h.

of DLS is biased toward the detection of large colloids, resulting in inaccurate size distributions in polydisperse systems.[34]

To compare the evolution of the PPh_3-protected Au clusters in different primary alcohols, methanol is replaced with ethanol, which has a slower reaction rate coefficient with $NaBH_4$ (Figure 3).[24,26] After $t_{react} \approx$ 30 min, an almost featureless absorbance spectrum is observed in UV−vis measurements with only a small formation of a shoulder apparent centered near 550 nm. The shoulder is red-shifted relative to the methanol mixtures indicating larger species present in solution, based on surface plasmon resonances of gold nanoparticles.[30,35] Although the ethanol solution does not initially reveal a distinct absorbance feature, a strong blue-shifted shoulder centered ∼475 nm becomes discernible after 9 days (Figure 3e).

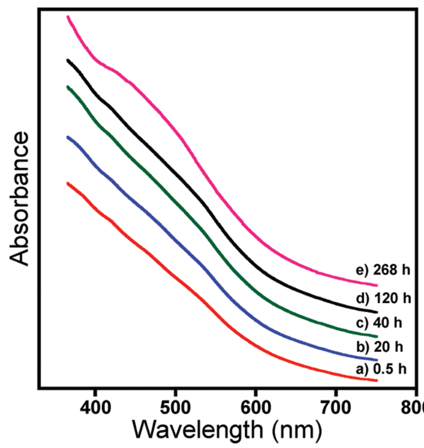

Figure 3. UV−vis spectra of PPh_3-protected Au clusters in 1:1 ethanol/chloroform solutions from t_{react} = 0.5 h to t_{react} = 268 h. The synthesis solutions show broad, weakly defined absorption bands making specific cluster nuclearities difficult to monitor.

Preparation and Characterization of $[Au_6L^3{}_4]^{2+}$ Clusters. An essential step for developing a validated colorimetric assay is the identification of the target species that undergo chemical conversion into measurands possessing distinct UV−vis spectra. The colorimetric assay that we fully develop in the following three sections samples a large range of MPC sizes, resulting in the production of two measurands. One measurand, $[Au_6L^3{}_4]^{2+}$, is not spectroscopically characterized nor is its synthesis from $AuClPPh_3$ reported. We provide this critical information here.

van der Velden, *et al.*[36] reported the preparation of $[Au_6L^3{}_4](NO_3)_2$ by reacting $[Au_9(PPh_3)_8]^{3+}$ in 20× molar excess L^3:Au solution, and the synthesis product was characterized by X-ray crystallography, and ^{197}Au Mössbauer and $^{31}P\{^1H)$ NMR spectroscopies.[37] The UV−vis spectrum was not reported; however, the authors noted that CH_2Cl_2 solutions containing $[Au_6L^3{}_4]^{2+}$ are "a very intense blue" and produce clear, bright red crystals.[36] The stability of this cluster is discussed by Evans and Mingos.[38] More recently, Hudgens, *et al.* reported the transient formation of $[Au_6L^3{}_4]^{2+}$ by the reduction of unequilibrated $AuClPPh_3$ and L^3 in 1:1 methanol/chloroform. They observed blue solutions of λ_{max} = 585 nm that yielded red crystals when infused with diethyl ether; however, a reliable synthesis method was not developed.[31]

The current study develops and utilizes a reliable one-pot synthetic procedure for the production of $[Au_6L^3{}_4]^{2+}$ clusters. Our synthesis scheme starts after the reduction of $AuClPPh_3$ to form a solution containing PPh_3-ligated Au_8 and Au_9 species, as is shown in Figure 4A (trace a) and Figure 4B (trace a). The solution was prepared by dissolving $AuClPPh_3$ and $NaBH_4$ in 1:1 methanol/diethyl ether and allowing the solution to react until t_{react} = 48 h; it is the same solution as shown in Figure 2A. The reaction solution exhibits a strong

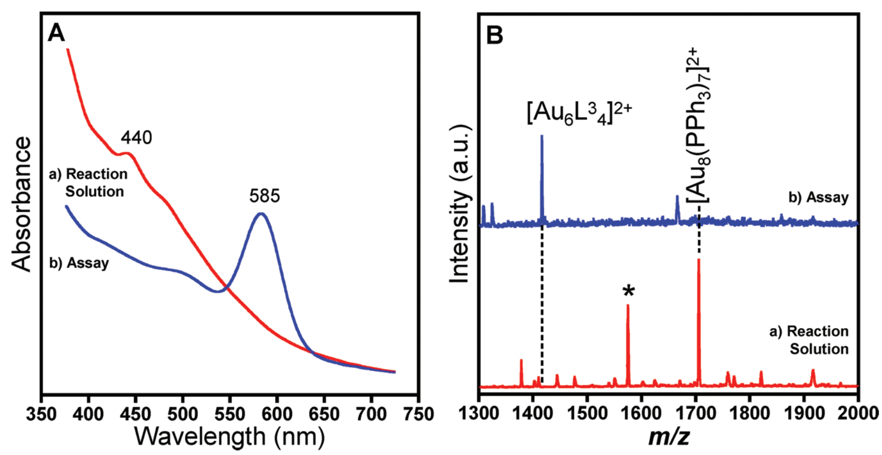

Figure 4. (A) UV−vis spectra and (B) ESI-MS spectra of reduced gold solutions prior to and after addition of excess L^3 ligands (assay) in 1:1 methanol/diethyl ether solvent mixture shows the formation of $[Au_6L^3{}_4]^{2+}$ from both PPh_3-protected Au_8 and Au_9 clusters. The transformation of ligated Au_9 species to $[Au_6L^3{}_4]^{2+}$ is characterized by the loss of 440 nm absorption and growth of the 585 nm absorption band. Similarly, the ESI-MS signal transitions from Au_8 clusters to $[Au_6L^3{}_4]^{2+}$ (*m/z* 1416). The (*) in panel B denotes $[Au_8(PPh_3)_6]^{2+}$, which is a CID fragment produced from $[Au_8(PPh_3)_7]^{2+}$, indicating the sum of the Au_8 peaks more accurately represents the $[Au_8(PPh_3)_7]^{2+}$ population. See text for more details.

absorption band at 440 nm (Figure 4A), which we previously assigned as Au_9 species, where the cluster complex may be charged or neutral. Furthermore, the ESI-MS spectrum of the reaction solution displays a strong $[Au_8(PPh_3)_7]^{2+}$ peak and a diminutive $[Au_8(PPh_3)_6]^{2+}$ peak (Figure 4B), which is an in-source, collision induced dissociation (CID), secondary fragment.[39]

Addition of a 3× molar excess of L^3 to the solution initiates ligand exchange reactions on the Au clusters. Equilibrium studies in chloroform solutions have shown that L^3 binds more strongly with Au^I than PPh_3,[1] and complete ligand exchange of PPh_3 on the clusters is experimentally determined to occur at the 3× molar excess (not shown). (Note: The addition of greater molar excess amounts of L^3 results in further degradation of the cluster distribution into smaller clusters and complexes. The colorimetric assay was not optimized for higher molar concentrations of PPh_3.) Twenty-four hours after L^3 is added to the solution in an unstirred reaction vial, its UV−vis spectrum exhibits a strong λ_{max} = 585 nm, and the 440 nm absorption band has completely diminished (Figure 4A). Note, the reaction occurs within a few hours in sealed, stirred reaction vials. The solution color has become an intense blue. During the reaction the absorption band remains centered at 585 nm, indicating the absorption band originates from a specific product and is not an effect of aggregation. The ESI-MS data (Figure 4B) support the identification of a single product on the basis that a single peak emerges at 1416 *m/z*, which corresponds to $[Au_6L^3{}_4]^{2+}$. The emergence and growth of the 1416 *m/z* peak is concomitant with the depletion and complete removal of the $[Au_8(PPh_3)_7]^{2+}$ peak. Thus, these data indicate that $[Au_9(PPh_3)_y]^{z+}$ and $[Au_8(PPh_3)_7]^{2+}$ react to form $[Au_6L^3{}_4]^{2+}$, which shares the same structure as reported by Van der Velden, *et al*.

Although UV−vis and ESI-MS detect the production of $[Au_6L^3{}_4]^{2+}$ from $[Au_8(PPh_3)_y]^{z+}$ and $[Au_9(PPh_3)_y]^{z+}$, these data are insufficient to confirm that the conversion reaction has reached completion. DLS can monitor the colloids that consist of primary clusters that are available for reaction, and it can also determine if a significant fraction of colloids remain. In short, the addition of 3 x molar excess L^3 optimized the transformation of the agglomerated primary clusters to stable species, indicated by the inability of the DLS to measure any distribution. The DLS also provides more defined limits for development of the assay (*vide infra*). The DLS data and experimental description can be found in the Supporting Information (Figure S1).

The $[Au_6L^3{}_4]^{2+}$ is fragile in uncapped solutions on the benchtop, consistent with our previous observations. It can be stored refrigerated for weeks, and it remains stable in sealed vials in the dark.[31] In an unstirred vial, $[Au_6L^3{}_4]^{2+}$ shows that the degradation of the blue colored solution to a pale yellow solution occurs in less time for solutions prepared with shorter reduction (t_{react}) times, that is, the time after $NaBH_4$ is added to the dissolved $AuClPPh_3$ precursor solution, prior to the addition of L^3. As the reduction time is increased, the blue color persists for longer periods, indicating that the concentration of $[Au_6L^3{}_4]^{2+}$ determines the duration of the blue color. Furthermore, $[Au_6L^3{}_4]^{2+}$ is photoactive. When exposed to natural sunlight, blue solutions that display an intense 585 nm absorption band and a prominent $[Au_6L^3{}_4]^{2+}$ ion peak, rapidly fade to the pale yellow color. The ESI-MS data obtained from bleached solutions do not exhibit a $[Au_6L^3{}_4]^{2+}$ peak, evidencing its photodecomposition. Thus, to preserve the $[Au_6L^3{}_4]^{2+}$ measurand, the results presented here were obtained in dark conditions or vials covered with foil until ready for examination.

Measurement of $[Au_8(PPh_3)_y]^{z+}$ and $[Au_9(PPh_3)_y]^{z+}$ by Colorimetric Assay. As reported by van der Velden *et al.*,[36] L^3 ligands completely replace PPh_3 on the surface of $[Au_9(PPh_3)_8]^{3+}$ clusters through ligand exchange, forming $[Au_6L_4]^{2+}$. This process suggests the net reaction:

$$[Au_9(PPh_3)_8]^{3+} + 4L^3 \rightarrow [Au_6L^3{}_4]^{2+} + 3[Au(PPh_3)_2]^{+} + 2PPh_3 \quad (1)$$

In the development of the one-pot synthesis of the $[Au_6L^3{}_4]^{2+}$ species, strong experimental evidence supports other formation pathways besides the L^3 exchange with $[Au_9(PPh_3)_8]^{3+}$ in reaction 1. Upon L^3 addition the strong $[Au_8(PPh_3)_7]^{2+}$ peak diminishes. Concurrently, the $[Au_6L^3{}_4]^{2+}$ peak grows (Figure 4); therefore, PPh_3-protected Au_8 and Au_9 clusters should both have reaction pathways to form $[Au_6L^3{}_4]^{2+}$.

The transformation of both PPh_3-protected Au_8 and Au_9 clusters to $[Au_6L^3{}_4]^{2+}$ provides a tool to temporally probe the size distribution of these clusters. Precedence for product formation involving ligated Au_8 and Au_9 species exists. Identical ligated Au_9 products are formed *via* reactions between isopropyl isocyanide and $[Au_8(PPh_3)_7]^{2+}$ or $[Au_9(PPh_3)_8]^{3+}$ clusters; the ligated Au_9 products were characterized by crystal structure analysis.[40] The formation of similar products can be attributed to the L^3- or PPh_3-promoted disproportionation of $[Au_9(PPh_3)_8]^{3+}$ to $[Au_8(PPh_3)_7]^{2+}$ and $[Au(PPh_3)_{2-n}(L^3)_n]^{+}$ ($0 \leq n \leq 1$), which has previously been reported for PPh_3-protected Au clusters.[41] Because the fast reduction reactions with the Au precursor and $NaBH_4$ initially form neutral species in the current synthetic procedures,[31] reaction pathways for the formation of $[Au_6L^3{}_4]^{2+}$ should include neutral, ligated Au_8 and Au_9 clusters. Low barriers to charge exchange may render the reaction network relatively independent of charge states. For example, cationic $[Au_9(PPh_3)_8]^{z+}$ (z = 1, 2, 3) clusters are known to have small barriers to charge exchange.[42] Reactions involving the degradation of ligated Au_8 clusters to $[Au_7(PPh_3)_7]^{+}$

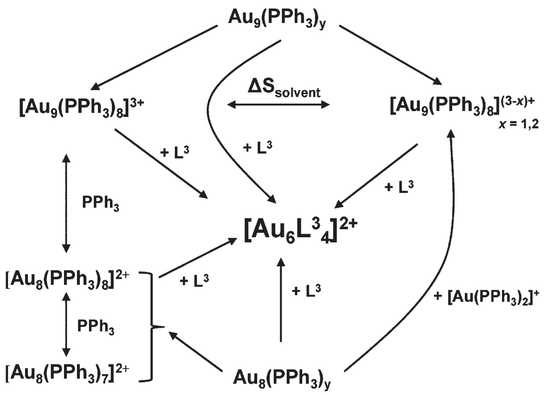

Scheme 1. Transformation of neutral and ionic PPh_3-protected Au_8 and Au_9 clusters to $[Au_6L^3{}_4]^{2+}$.

are reportedly not observed in excess PPh_3 solutions and are assumed to have no role in the reaction scheme;[43] therefore, Scheme 1 is developed to summarize the reactions that form $[Au_6L^3{}_4]^{2+}$ *via* L^3 addition to Au_8 and Au_9 clusters. Note, the reactions resulting in the formation of $[Au_6L^3{}_4]^{2+}$ *via* L^3 addition are predicted to have large equilibrium coefficients, indicating almost no reverse reaction. Thus, after application of the colorimetric assay (described in the experimental section), the integrated area of the 585 nm absorption band, $W(\{Au_8,Au_9\}_{585\ nm})$, provides a measure of the PPh_3-protected Au_8 and Au_9 clusters at t_{react}.

Measurement of $[Au_{10}(PPh_3)_y]^{z+}$ and $[Au_{11}(PPh_3)_y]^{z+}$ by Colorimetric Assay. Facile, complete ligand exchange on PPh_3-protected clusters with L^3 creates an opportunity for probing not only neutral and ionic Au_8 and Au_9 species, but also the primary Au_x MPCs with nuclearity $x \geq 10$. L^3 protected clusters have a propensity to form $[Au_{11}L^3{}_5]^{3+}$, which has a characteristic λ_{max} = 420 nm.[1,2] Ligated Au_{10} species (*e.g.*, $[Au_{10}L^6{}_4]^{2+}$, L^6 = 1,6-bis(diphenylphosphino)hexane) also exhibit an absorption maximum centered near 420 nm;[1,2,13,28,31,32,44] thus, the integrated absorption of the 420 nm band is a rough estimate of the weights of PPh_3-protected Au_x clusters of nuclearity $x > 9$. Application of the colorimetric assay to aliquots of the reaction solution will improve the measurement accuracy because L^3-protected Au_{11} species are reported to form through an addition reaction with PPh_3-protected Au_{10},[31] suggesting that reactions within the colorimetric assay will convert PPh_3-ligated Au_{10} to the L_3-ligated Au_{11} measurand. Therefore, when the solution contains only PPh_3-protected members of the set, $\{Au_{10}, Au_{11}\}$, reactions in the presence of excess L^3 will yield a 420 nm band that has the integrated intensity, $W(\{Au_{10}, Au_{11}\})_{420\ nm}$, that is exactly proportional to the concentration of PPh_3-ligated clusters in the sample aliquot that are converted to $[Au_{11}L^3{}_5]^{3+}$.

We note that the integrated intensity determination around 420 nm absorption band may contain contributions of larger Au_x ($x \geq 10$) clusters that absorb within the absorption band envelope. For example, the ligated Au_{13} cluster, $[Au_{13}Cl_2(PMe_2Ph)_{10}]^{3+}$ (PMe_2Ph = dimethylphenylphosphine), exhibits a weak absorption tail under the 420 nm absorption band of $[Au_{11}L^3{}_5]^{3+}$; consequently, we may expect phosphine-protected Au_{13} species to contribute to the integrated area of the 420 nm band.[32,44] Thus, we deduce that an absorption band measured at 420 nm can reflect the relative concentrations of phosphine-ligated Au_x ($x \geq 10$) species. Although we cannot define the set $\{Au_x: x \geq 10\}$ exactly, additional data obtained during experiments can help deduce the upper limit of nuclearity (*vide infra*).

Formal Description of the Colorimetric Assay. The identification of two specific bin sizes can now be developed through the complete ligand exchange reactions of PPh_3-protected clusters with L^3 classified by the sets: $\{Au_8,Au_9\}$ and $\{Au_x: x \geq 10\}$. The amount of the assay reagent, L^3, is optimized to completely exchange the PPh_3, but not degrade product distributions. Knowledge that the blue colored product is $[Au_6L^3{}_4]^{2+}$ allows for the development of schemes that probe the $[Au_x(PPh_3)_y]^{z+}$ (x = 8, 9) nuclearity distribution of PPh_3-protected Au_x clusters, as compared with $[Au_x(PPh_3)_y]^{z+}$ ($x \geq 10$). The method uses the colorimetric assay procedure described in the experimental section to consolidate an ensemble of PPh_3-protected gold cores into two sets: (1) population of the set, $\{Au_8, Au_9\}$, that is proportional to $W(\{Au_8, Au_9\})_{585\ nm}$, which is evaluated by measuring the integrated absorbance of the 585 nm band, and (2) population of the set, $\{Au_x: x \geq 10\}$ that is proportional to $W(\{Au_x: x \geq 10\})_{420\ nm}$, which is evaluated by measuring the integrated absorbance of the 420 nm band. As described above, the integration process of the absorption band centered at 420 nm predominantly measures the weight of $\{Au_{10}, Au_{11}\}$; however, contributions from larger clusters are also considered (*vide infra*). To reduce the clutter of the present terminology, we introduce the equivalence symbols: $W^{8,9}_{585nm} \equiv W(\{Au_8, Au_9\})_{585\ nm}$ and $W^{x\geq 10}_{420\ nm} \equiv W(\{Au_x: x \geq 10\})_{420\ nm}$. The method allows for qualitative and some quantitative information on *both* the cluster distribution and population density as a function of t_{react}.

Examination of PPh_3-Protected Au Cluster Evolution with Colorimetric Assay. Application of the colorimetric assay to aliquots of reaction solutions can characterize the distribution and population of PPh_3-protected cluster nuclearities of $\{Au_8, Au_9\}$ and $\{Au_x: x \geq 10\}$, as a function of time, t_{react}. Figure 5A shows UV−vis spectra as a function of t_{react} for colorimetric assays collected from aliquots of the 1:1 methanol/diethyl ether synthesis. Integration of the absorption bands yields $W^{8,9}_{585nm}$ and $W^{x\geq 10}_{420nm}$ for each t_{react}. Figure 5B plots the fractional weight percents of $W(\{Au_8, Au_9\}_{585\ nm}) / \Sigma_i W_i$ and $W(\{Au_x: x \geq 10\}_{420\ nm})/\Sigma_i W_i$, computed from each

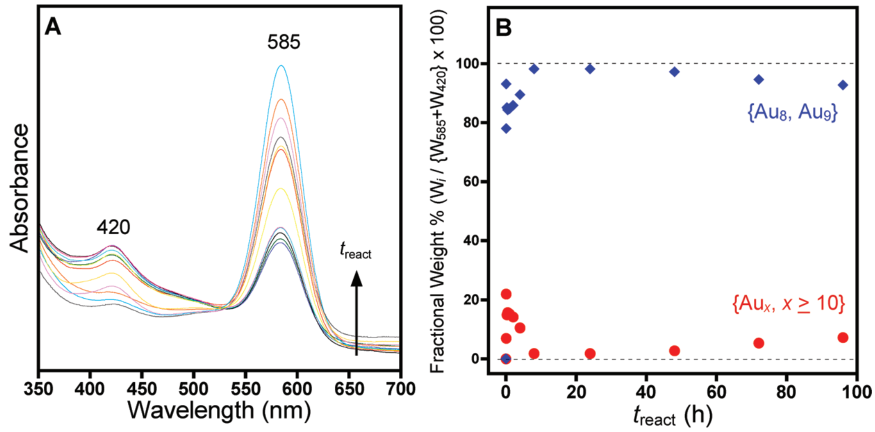

Figure 5. (A) UV−vis spectra taken from t_{react} = 0−96 h and (B) the relative intensities of the 420 nm (red dot) and 585 nm (blue diamond) absorption bands representing {Au_x: $x \geq 10$} and {Au_8, Au_9} size bins, respectively, in 1:1 methanol/diethyl ether solutions. The relative band weights, W_i, are monitored with UV−vis as a function of time after the addition of the assay reagent, L^3.

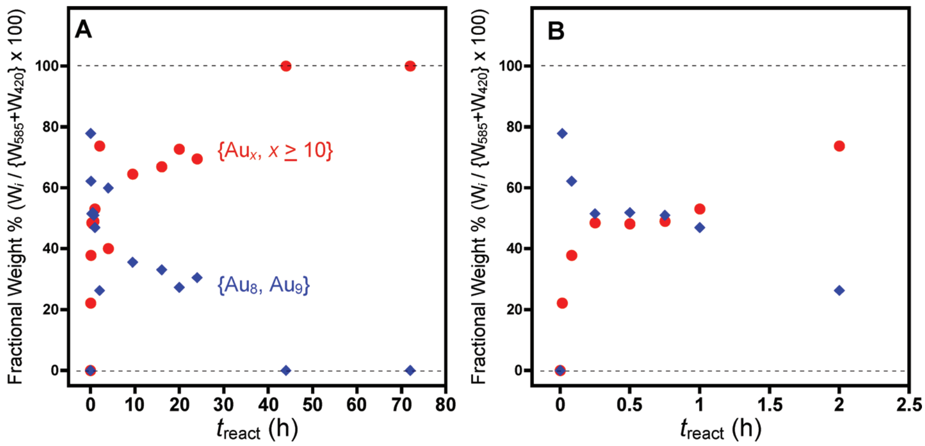

Figure 6. (A) The relative intensities of the 420 nm (red dot) and 585 nm (blue diamond) absorption bands representing {Au_8, Au_9} and {Au_x: $x \geq 10$} size bins, respectively, in 1:1 ethanol/diethyl ether solutions from t_{react} = 0 h to t_{react} = 72 h after L^3 addition and (B) magnified view of the first 2.5 h. The disappearance of the 585 nm absorption band by t_{react} = 72 h indicates almost complete depletion of the {Au_8, Au_9} ligated cores from solution.

trace of Figure 5A. The term, $\Sigma_i W_i$, is the sum of the integrated intensities, and $W_{420nm}^{x\geq 10}$ at each t_{react}. The initial evolution of the fractional weight percents up to t_{react} = 8 h is plotted in Supporting Information, Figure S2.

Initially at $t_{react} \approx$ 1 min, a large percentage (W({Au_8, Au_9}$_{585\ nm}$) /$\Sigma_i W_i$ > 90%) of the total integrated area is attributed to $W_{585nm}^{8,9}$ (Figure 5B and Supporting Information, Figure S2). An immediate decrease in the $W_{585nm}^{8,9}$ is observed at t_{react} = 5 min. After t_{react} = 5 min, steady growth of the $W_{585nm}^{8,9}$ continues up to t_{react} = 8 h (Figure 5B). The nascent high concentration of $W_{585nm}^{8,9}$ that was immediately diminished at t_{react} = 5 min is likely an artifact due to incomplete mixing. The $W_{420nm}^{x\geq 10}$ at t_{react} = 8 h is almost depleted, consistent with the continual growth of $W_{585nm}^{8,9}$. Examination of the relative concentrations of the two sets, {Au_8, Au_9} and {Au_{10}, Au_{11}}, becomes useful for describing the evolution of the PPh_3 protected clusters by examining their relative intensities as a function of time. A clear growth in the $W_{585nm}^{8,9}$ is observed up to t_{react} = 8 h and concurrent with the steady decrease in $W_{420nm}^{x\geq 10}$. In this study we observe after t_{react} = 8 h, relative growth of $W_{420nm}^{x\geq 10}$, that can be interpreted as growth of larger clusters from {Au_8, Au_9} species, or alternately, as degradation from larger clusters that cannot be monitored by UV−vis. Evidence for growth of larger gold clusters from ionic phosphine-protected Au_8 or Au_9 clusters is reported.[28,44,45]

Application of the colorimetric assay to PPh_3-protected Au cluster formation in a stirred 1:1 ethanol/diethyl ether synthesis solution between $t_{react} \approx$ 1 min to t_{react} = 72 h is presented in Figure 6 and Supporting Information, Figure S3. At $t_{react} \approx$ 1 min both {Au_8, Au_9} and {Au_x: $x \geq 10$} are observed with $W_{585nm}^{8,9}$ constituting ~80% of $\Sigma_i W_i$, indicating the presence of a polydisperse product distribution. The set {Au_x: $x \geq 10$} increases relative to {Au_8, Au_9} until t_{react} = 15 min, where almost equivalent $W_{585nm}^{8,9}$ and $W_{420nm}^{x\geq 10}$ is observed. The $W_{585nm}^{8,9}$ and $W_{420nm}^{x\geq 10}$ remain similar up to t_{react} = 1 h, where the $W_{420nm}^{x\geq 10}$ begins to dominate the

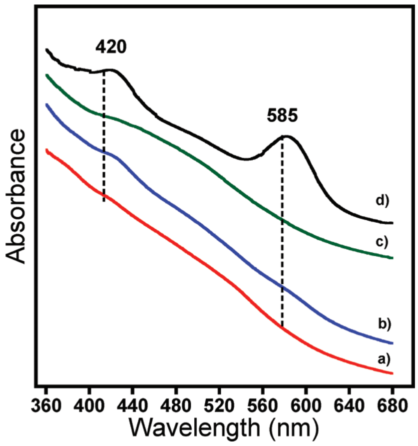

Figure 7. UV−vis spectra of 1:1 ethanol/diethyl ether solutions containing equimolar $AuClPPh_3$ and $NaBH_4$. (a) Solution of equimolar $AuClPPh_3$ and $NaBH_4$ at t_{react} = 72 h (3 days); (b) colorimetric assay of the reaction solution at t_{react} = 72 h (3 days); (c) solution of equimolar $AuClPPh_3$ and $NaBH_4$ at t_{react} = 216 h (9 days); and (d) colorimetric assay of the reaction solution at t_{react} = 216 h (9 days). The enhanced 420 and 585 nm absorption bands at t_{react} = 216 h (9 days) evidence that ligated members of the sets, $\{Au_8, Au_9\}$ and $\{Au_x: x \geq 10\}$, are again present in solution.

UV−vis spectrum of the assayed reaction solution clearly depicted in Figure 6B. At $t_{react} > 1$ h, the colorimetric assay shows $\{Au_8, Au_9\}$ are significantly diminishing in the reaction solution. The set $\{Au_8, Au_9\}$ continues to steadily decline and is completely diminished at t_{react} = 72 h, indicated by an inability to discern $W^{8,9}_{585nm}$ from the UV−vis background (Figure 6 and Supporting Information, Figure S3). With the decreasing $\{Au_8, Au_9\}$, the $\{Au_x: x \geq 10\}$ increases until $t_{react} \approx$ 44 h. At $t_{react} > 44$ h, the relative population of $\{Au_x: x \geq 10\}$ diminishes, indicated by a decrease in the overall $\Sigma_i W_i$ (not shown).

The absence of $W^{8,9}_{585nm}$ and greatly diminished $W^{x\geq10}_{420nm}$ by $t_{react} \approx 72$ h (Figure 6A) is more clearly depicted by comparing the UV−vis spectra of the test and assayed reaction solutions, as shown in Figure 7. In Figure 7 trace (a) presents the UV−vis spectra of the reaction solution at t_{react} = 3 days, and trace b presents the UV−vis spectrum of this reaction solution after the application of the colorimetric assay. Neither the assayed solution nor the reaction solution exhibit easily discernible $W^{8,9}_{585nm}$ and $W^{x\geq10}_{420nm}$ at t_{react} = 3 days, indicating that the solution contains few, if any, ligated Au_x ($8 \leq x \leq 13$) clusters. Moreover, the colorimetric assay solution (Figure 7, trace b) exhibits almost no optical fingerprint, even though the solution remains dark, indicating the strong presence of larger ligated Au species. At t_{react} = 9 days the reaction solution is relatively featureless (Figure 7, trace c), the colorimetric assay of this solution (Figure 7, trace d) exhibits the reappearance of $W^{8,9}_{585nm}$ and $W^{x\geq10}_{420nm}$, indicating the presence of PPh_3-protected Au_x ($8 \leq x \leq 11$) clusters (and an unknown amount of Au_x, $x > 11$ clusters). These UV−vis bands arise from the degradation of larger phosphine-protected Au_x: $x > 11$ clusters. The reemergence of these smaller clusters could arise *via* stepwise growth of smaller cluster species, but this mechanism is improbable because the current system can monitor species below Au_x: $x \leq 13$, and no experimental data from the test or assayed reaction solutions (*i.e.*, UV−vis, ESI-MS, or DLS) provide evidence of such growth.

The experimental data evidencing the evolution of the PPh_3 cluster distribution allow us to better define the limits of the size bin, $\{Au_x: x \geq 10\}$. In the ethanol solvent systems at t_{react} = 3 days, almost no PPh_3-protected clusters were present in the assayed reaction solution, but the solution remained dark, indicating the presence of colloids. We can distinguish phosphine-protected Au clusters with nuclearity, Au_x: $x \leq 13$. Ligated Au_{25} clusters and larger nanoparticles are reported to have optical fingerprints observable in the UV−vis spectra,[35,46] but we do not see such characteristic UV−vis features. Because we have a well-established experimental range which can be well characterized with UV−vis measurements, we surmise that the black ethanol synthesis solution, which has a measured DLS distribution, comprises colloids containing agglomerated, ligated $\{Au_x: 13 < x < 25\}$; therefore, we can assign a less ambiguous upper limit to the $\{Au_x: x \geq 10\}$ and reassign $W^{x\geq10}_{420nm}$ to $W(\{Au_x: 10 \leq x \leq 13\})_{420nm} \equiv W^{10\leq x\leq13}_{420nm}$. The assignment of the upper size limit for the larger size bin also allows better characterization of the cluster distribution, especially in methanol solvent systems. The DLS instrument has a reported lower size limit for detection near ∼1 nm, making the technique amenable to phosphine-protected clusters larger than Au_{13}. With the absence of a measurable population of colloids in the DLS, nearly the entire cluster distribution is captured by the $W^{8,9}_{585nm}$ and $W^{10\leq x\leq13}_{420nm}$ in the methanol solvent systems that display no DLS signatures. The better defined upper limit allows the more accurate description of the assayed (L^3 protected) Au clusters present in synthesis solutions.

The application of our colorimetric assay allows the deconvolution of broad UV−vis spectra similar to those reported in Figures 1, 2A, and 3, which do not allow clear distinction between different phosphine-protected Au clusters. Although coupling DLS and UV−vis measurements of reaction solutions, as employed in the current study (Figure 2), allow for some qualitative interpretation of Au cluster size evolution, clear distinction of specific clusters involved in formation reactions cannot be deduced. The implementation of the colorimetric assay allows us to probe nearly the entire ligated Au cluster distribution and to compare the evolution in methanol and ethanol solvent mixtures. Because reaction conditions and alcohol/diethyl ether concentrations are almost identical, the cluster population and distribution should directly be a function of the different reduction rates of Au^I by

NaBH$_4$ in methanol and ethanol solvent systems. The disappearance of the $W^{8,9}_{585nm}$ from 1:1 ethanol/diethyl ether solution and subsequent formation of larger clusters not amenable to UV−vis measurements is in stark contrast to the 1:1 methanol/diethyl ether solution, where both $W^{8,9}_{585nm}$ and $W^{10\leq x\leq 13}_{420nm}$ persist and fully describe the entire cluster ensemble throughout the time period monitored. The differences in the growth and formation pathways of the phosphine-protected gold clusters in methanol and ethanol systems allow the development of a more complete description of the role for PPh$_3$ in size-selective syntheses.

Experimental evidence for phosphine-protected Au$_x$ cluster etching in the presence of PPh$_3$ is supported in all reaction systems in the current study. As previously described, PPh$_3$-protected Au$_x$: $x > 13$ clusters dominate the cluster distribution at $t_{react} = 3$ days in ethanol solvent systems. The subsequent reappearance of {Au$_8$, Au$_9$} and {Au$_x$: $10 \leq x \leq 13$}, as detected by the colorimetric assay provides compelling evidence that larger cluster species, Au$_x$: $x > 13$, are susceptible to PPh$_3$ etching (Figure 7). Direct evidence for Au$_x$ cluster etching can be observed in the methanol synthesis solutions. Initially, a polydisperse distribution of clusters is observed, but by $t_{react} = 8$ h the {Au$_x$: $10 \leq x \leq 13$} size bin is depleted (Figure 5), and DLS measurements do not report the presence of any larger species in solution; therefore, the etching of the {Au$_x$: $10 \leq x \leq 13$} results in a monodisperse cluster distribution that contains almost exclusively {Au$_8$, Au$_9$}. UV−vis spectra of nonassayed and assayed reaction solutions both report growth of distinct optical features representative of ligated Au$_8$ (Figure 1) and ligated Au$_9$ clusters (Figure 2) in methanolic solvent systems, respectively. The data taken collectively from methanol and ethanol solvent systems describe ubiquitous etching of multiple {Au$_x$: $8 \leq x < 25$} clusters.

Theoretical and experimental studies examining the role of PPh$_3$-protected Au cluster production and stabilization with conflicting results. Part of the conflict may reside in computational methods. To minimize computational costs, many theoretical studies directed at the formation and stabilization of phosphine protected gold clusters treat PPh$_3$ as phosphine (PH$_3$). The simplification has been proven useful for structural determination,[47] but it can lead to discrepancies with experiment due to an inability to capture the electronic contributions of PPh$_3$.[47,48] The phenyl groups on PPh$_3$ are strong electron withdrawing groups creating a positively charged phosphorus capable of accepting back-donation from the cluster core. The stabilizing metal to ligand π back bonding describes a localization of charge. Experimentally, a diphosphine derivative, where a phenyl ring was replaced by an ethyl group, showed differences in both the final product formation and product dispersity.[49] Density functional theory calculations described the phosphorus with two phenyl groups to be more positive than the ethyl derivative. Examination of the effect of ligation (PH$_3$) on the stability of Au$_{13}$ clusters reports a transition from a tightly bound 2D configuration for bare clusters to a 3D icosahedral structure for the ligated system where Au−Au bond lengths are much longer and redistributions of charge to Au-PH$_3$ bond occur.[50] The elongation of the Au−Au bonds is reportedly due to the repulsion of the more positively charged Au atoms caused by the charge transfer to the Au−P bonds, resulting in stronger coupling, covalent bonds. Extensive studies of metal−ligand complexation with phosphines for catalysis have reported the significance of the electronic and steric considerations of the phosphine ligand.[9,51,52]

This study reports the first direct experimental evidence that PPh$_3$ has the ability to etch nascent, ligated Au clusters in synthesis solutions containing equimolar Au and PPh$_3$. The extent of processing increases with increasing concentrations of PPh$_3$ in both aerated and deaerated systems, supporting the thesis that phosphine ligands are the main driving force for cluster formation instead of free halides or oxidative agents. This is further supported by observing that increasing the molar excess of PPh$_3$ in methanolic solutions promotes growth to larger clusters (Supporting Information, Figure S4). This result is consistent with Figure 5 in the main text, showing growth from a PPh$_3$-ligated Au$_8$ and Au$_9$ platform.

The previous two studies describing the importance of the electronic structure of the phosphine ligands and Au cluster formation are consistent with the description of PPh$_3$ as more than a place holder.[49,50] Specific Au$_x$ clusters show increased resistance to PPh$_3$ etching, promoting the formation of narrower product distributions. Combining the current results with our previous reported degradation of specific phosphine-protected Au clusters that form monodisperse products[28] allows the description of PPh$_3$ as both a protective and etching agent to be a general description for phosphine ligands with similar electronic structure.

Mechanistic Implications for PPh$_3$ Etching. Etching during TM cluster evolution is driven by free energy considerations of stable clusters, and its incidence strongly depends on the nature of the nascent cluster distribution formed through the kinetically driven reduction of the Au:ligand complex precursors:

$$\mathrm{Au^IPPh_3Cl} + e^- \xrightarrow{k_1} [\mathrm{Au^0PPh_3Cl}]^- \qquad (1)$$

$$[\mathrm{Au^I(PPh_3)_2}]^+ + e^- \xrightarrow{k_2} [\mathrm{Au^0(PPh_3)_2}] \qquad (2)$$

where reactions 1 and 2 are characterized by rate coefficients, k_1 and k_2, which are assumed to be fast. The production of ligated Au^0 species produces a supersaturated solution. Nucleation processes spontaneously occur when the change in free energy, ΔG, of the system, driven by the supersaturation of the nucleating species, exceeds the barrier for phase change. The formation of stable products occurs when the size of the nascent product sufficiently lowers the total free energy to counterbalance the newly formed surface energy. The product size where balance is achieved is defined as the critical nucleus, r^*. Above the critical nucleus, the cluster is stable and growth is thermodynamically favored. Below the r^*, the cluster will be unstable and dissociate back into solution complexes. Nucleation persists until the supersaturated solution becomes depleted, $d\Delta G/dr = 0$, and surface growth subsequently occurs. At $d\Delta G/dr = 0$, where growth is classically expected, the current study provides strong evidence that competing reactions between growth and etching are present. This feature of product formation has not been implemented into models describing ligand-protected TM cluster formation.

Competition between growth and etching reactions is clearly observed during gold cluster syntheses in methanol/diethyl ether solvent (Figure 5). Initially, a polydisperse distribution of clusters forms, indicated by significant populations of both $\{Au_8, Au_9\}$ and $\{Au_{10}, Au_{11}\}$ clusters. Subsequent degradation of the $\{Au_x: 10 \leq x \leq 13\}$ is observed until $t_{react} \approx 8$ h, indicating that the etching reaction rate dominates the growth rate; thus, a monodisperse distribution of stable, ligated Au clusters forms through the reaction:

$$Au_{(n^*+b)+m} \xrightarrow{k_3,\,\text{etch}} Au_{n^*+b} + mAu \qquad (3)$$

where reaction 3 represents the etching process with a rate coefficient, k_3, n^*+b is the number of Au atoms for the most stable cluster larger than r^* (r^* cannot be explicitly determined in the current study), and n^* replaces r^* because nuclearity can be accurately determined. After $t_{react} \approx 8$ h, the reappearance of $\{Au_x: 10 \leq x \leq 13\}$ is observed. Because the colorimetric assay can bin nearly the entire cluster distribution (*vide supra*) and no significant population of clusters larger than Au_{13} are present, the reemergence of $\{Au_x: 10 \leq x \leq 13\}$ at $t_{react} > 8$ h is described by stepwise growth reactions:

$$Au_{(n^*+b)} + mAu \xrightarrow{k_4,\,\text{growth}} Au_{(n^*+b)+m} \qquad (4)$$

where k_4 is the (global) growth rate coefficient of the ligated clusters.[53] When etching reaction 3 is active, the competing growth reaction 4 completes a loop around the most thermodynamically stable ligated cluster, $Au_{(n^*+b)}$. After a sufficient population of ligated $Au_{(n^*+b)}$ clusters have formed through reaction 3, $t_{react} \leq 8$ h, the net growth rate exceeds the etching rate, promoting the formation of larger clusters, as described in reaction 4 and observed in Figure 5 after $t_{react} \approx 8$ h. The more stable clusters, $Au_{(n^*+b)}$, have greater resistance to etching and growth, allowing their accumulation. Similar cyclic processing in ethanol solvent systems is observed; therefore, we formally define this cyclic processing around the most stable cluster as "size-selectivity".

Size-selective processing that forms monodisperse products is driven by the relative reaction rates for growth and etching. The cyclic processing around a specific Au cluster nuclearity promotes the formation of a monodisperse product which can also become a platform for growth.[28] Although the etching reaction rate (reaction 3) initially dominates in methanol solvent, the population of susceptible clusters diminishes and the growth rate begins to dominate cluster formation. The formation of "platform" clusters for subsequent product formation was first reported by our group for phosphine-protected Au clusters.[28] The size-selective methodology differs from the "size-focusing" methodology outlined for thiol ligands.[54] The principles for size-focusing are based solely on the resistance of specific cluster sizes to degradation, *e.g.*, ligand etching or oxidation, expressed by the coinage, "survival of the robustest". Thus far, the size-focusing methodology does not provide a clear description to explain selectivity, and optimization is achieved by forming nascent species of nuclearity greater or equal to the target cluster. Importantly, size-focusing techniques are useful for producing relatively monodisperse product distributions but likely limit the product yield, due to a unidirectional degradation pathway. The concept of size-selective processing creates a framework for more accurately describing other gold-ligand systems such as those involving amines, thiols, and other polymeric ligands that have roles in both cluster growth and etching processes.[4,7,55] The development of accurate reaction rate coefficients will require the development of other metrological techniques suitable for monitoring product evolution, and such research is ongoing in our lab. Still, the size-selective framework creates new opportunities for the optimization of synthetic processes.

General Framework of Size-Selective Processing. The development of accurate TM:ligand models that describe size-selective processing need to incorporate the pertinent growth and etching reactions and their corresponding rate coefficients. Understanding how to control the processing around the most stable clusters allows a direct method for producing *selective* products in monodisperse distributions through control of specific formation pathways. The elucidation and characterization of specific reactions (development of a reaction network) will diminish the need for iterative synthetic methods.

The formation of PPh_3-protected Au clusters can be described by a two-step nucleation and core growth formation mechanism. Reduction of the ligated Au^I species, outlined in reactions 1 and 2, produce free radical species.[31] The recombination reaction (nucleation) of the ligated Au^0 species produces predominantly nascent neutral clusters:

$$Au^0 + Au^0 \xrightarrow{k_{5,\text{ nucleation}}} Au^0{}_2 + (n* - 2)Au^0 \xrightarrow{k_{5,\text{ nucleation}}} AU^0{}_{n*} \quad (5)$$

where $k_{5,\text{nucleation}}$ is the global rate coefficient for the recombination reactions driving nucleation to ligated, stable clusters, $Au^0{}_{n*}$. Importantly, the reduction rates of the PPh_3:Au complexes are controlled by the reaction of $NaBH_4$ and alcohol solvent. The disparate nascent cluster nuclearities produced in different alcohol solvent systems may originate from differing reaction rates along like formation mechanisms or from changes in the reaction pathway, for example, diffusion limited or surface mediated formation mechanisms.

Gold cluster synthesis in methanol solvent systems quickly produces a large population of relatively small nuclearity clusters. Because the reaction rate at 298 K of $NaBH_4$ and methanol is fast ($t_{1/2}$ < 20 min) and competes with the reduction of Au^I complexes, the reducing environment, which drives reaction 5, should not persist for more than 1 h; therefore, we can confidently assign all product evolution after $t_{\text{react}} \geq 1$ h to core growth. Note, it is intractable to distinguish between growth and nucleation prior to the cessation of nucleation. The data in Figure 5 are consistent with the cessation of nucleation at $t_{\text{react}} \leq 1$ h, indicated by the presence of both $\{Au_8, Au_9\}$ and $\{Au_x: 10 \leq x \leq 13\}$. Growth and etching reactions dominate after depletion of the reducing environment at $t_{\text{react}} \geq 1$ h; therefore, as previously mentioned, the entire distribution of primary, ligated Au clusters is able to be binned, and it exhibits no DLS signature. In contrast, colloids constructed from aggregated primary clusters would not allow probing of individual clusters, and a D_h for the aggregates could be measured by DLS. The present data (Figure 5) evidence that the dark solutions consist of colloids comprising agglomerated primary clusters. Here, we define agglomeration only in the context of the IUPAC definition of weak, reversible interactions between primary clusters.[56] Subsequent cluster growth will proceed through diffusion-limited processes involving ligated Au^0 species that add to the ligated cluster core (reaction 4). The core growth process occurs on a similar time scale as the etching process (reaction 3) promoting cluster selectivity.

Ligated-gold cluster syntheses in ethanol solvent systems produce smaller concentrations of larger clusters. The reduction rate of Au^I is slower in ethanol, which is consistent with reported slower $NaBH_4$ and ethanol reaction rates.[26] In the current system the slower reduction rate and longer lifetime of the reducing environment in ethanol solvent systems make separation of nucleation and core growth schemes intractable; therefore, specifically identifying nucleation and core growth reactions are more difficult. The reduction potential of the active boron reducing species is expected to be similar for both methanol and ethanol solvent systems, suggesting that the nucleation pathway is similar in both solvent systems. In a recent review outlining work by Finke and co-workers, a general relationship between cluster size, R, and the relative rates of growth and nucleation are described by R = (growth rate)/(nucleation rate).[27] This relationship describes the nascent nucleation products observed in the current study, where smaller clusters are observed in the faster reducing (and nucleating) methanol solvent systems. Although, the general description describes the current data trends, other possible growth mechanisms other than diffusion limited growth may be controlling the formation of larger clusters in ethanol solvent systems.

Nucleation reaction rates are strongly dependent on the stability of the reduced species in the reaction media; therefore, the growth of larger clusters may be a product of surface-mediated growth processes, as is reported for other TM systems.[27,57−59] Previous studies examining the stability of different Au:ligand complexes and their subsequent reduction can provide insight in the growth mechanism present in the current system. Henglein and co-workers[60] reported the formation of reduced, free $[Au(CN)_2]^{2-}$ species in solution after reduction with hydrated electrons, which have a half-life of 1×10^{-4} s. Using similar reducing techniques, the reduction of cyanide protected gold complexes with the hydroxymethyl radical was later reported to form >10 nm nanoparticles in aqueous solutions, as measured with electron microscopy.[61] Importantly, an induction period was observed for the reduction with the alcohol radical.[61] The confirmation of an induction period was reported for $[Au(CN)_2]^-$ species, but the reduction potential of the alcohol radical was found to be insufficient.[62] The stability of the reduced gold complex containing strong field cyanide ligands should have similar stability to gold species complexed with more weakly bound chloride or PPh_3 ligands; therefore, free, ligated Au^0 complexes are able to be formed in the current ethanol/$NaBH_4$ systems. Moreover, the current data show that the time necessary to grow ligated clusters larger than Au_{13} is 3 days. This observation implies a growth rate that is too slow to support cluster formation *via* catalytic surface-mediated pathways because the necessary reducing environment would be depleted. Therefore, the formation mechanism including growth and etching processes most likely occur through a diffusion limited process in both alcohol solvent systems with $NaBH_4$.

The diffusion limited process for growth will be controlled by the distribution of nascent clusters because the etching reaction rates are dependent on the cluster size. The final product formation will strongly depend on the relative stability of each cluster nuclearity. In solution size-selective processing will occur around the most stable clusters. Because isolation of individual reaction steps is difficult, measurements of reaction rates for specific clusters will also be difficult. Instead, relative reaction rate information for the size-selective processing around the most stable species would provide sufficient information to model product formation. Temporal studies employing the present colorimetric assay make such relative rate measurements feasible.

CONCLUSIONS

The current study has examined the role of PPh_3 ligands during Au MPC formation in different synthesis environments. These experiments have identified dual roles for PPh_3 as a stabilizer and proactive etching agent. These conclusions are based upon results obtained using a useful colorimetric assay, developed by our group, that can evaluate the cluster size populations, $\{Au_8, Au_9\}$ and $\{Au_x\colon 10 \leq x \leq 13\}$. The application of the colorimetric assays in methanol and ethanol syntheses provides experimental evidence that growth and etching occur around the most stable cluster nuclearities, accounting for the narrowing of cluster dispersity. The colorimetric assay is not limited to studies of smaller clusters. It is currently being used to study degradation and growth mechanisms of larger cluster systems. Application to other solvents, mixed ligand systems, and ligand exchange processes are also being examined with the current or slightly modified colorimetric assay. The implementation of the assay supports our development of a formal definition for size-selective processing, which is characterized by monodisperse cluster formation through loops of competing etching and growth reactions around the most stable ligated clusters. This size-selective model is consistent with the observation of monodisperse product formation during our previous work with diphosphine-protected Au clusters. The differing stability and resistance to PPh_3 etching, displayed by different cluster sizes, indicate that specific reaction rates may vary as function of cluster nuclearity, but this study provides a more complete model for size-selective cluster formation as well as insight into the more general size-focusing methodology. The current study also provides a procedure for creating monodisperse, photoactive clusters, $[Au_6L^3{}_4]^{2+}$, which can be useful in numerous applications. Overall, the role of PPh_3 in the formation of stable clusters was found to *both* stabilize and etch Au clusters to specific sizes, indicating a more prominent role in the synthetic mechanism of MPCs than simply a place-holding surfactant.

METHODS

Mass Spectrometry. Mass spectrometric measurements were performed with a dual probe electrospray ion source, including an integrated three vacuum stage and ion optics assembly (Analytica of Branford),[63] coupled to a custom-built (by Ardara Technologies) Extrel CMS quadrupole mass spectrometer. Diluted syntheses solution samples were introduced to the ESI source *via* direct infusion (10 μL/min), and the source was purged with >1.0 mL of 1:1 methanol/chloroform solution between each sample. The precision of the fractional ion measurements of each species is $\leq$10% (2σ) based on five repeated measurements. Source conditions were optimized to maximize ion intensities while minimizing fragmentation. The potential difference between the capillary exit and the skimmer, also termed the in-source collision energy (CE), was usually set to 150 V but for quality purposes was occasionally varied from 20 to 250 V. Sample solutions were further diluted with 1:1 methanol/chloroform to produce stable ion currents.

Optical Characterization. Optical spectra of solutions were obtained using a Varian Cary II dual beam spectrometer. Dynamic light scattering (DLS) measurements were conducted using a Malvern Zetasizer Nano ZS equipped with a 4 mW 633 nm (He−Ne) laser at 298 K. Both instruments accepted the same quartz 1 cm path length cuvette. To remove domain-induced scattering of 1:1 methanol/chloroform solution, similar experiments were conducted in methanol/diethyl ether solutions for DLS measurements. The literature reports that the viscosity of diethyl ether is 0.224 cP,[64] and the manufacturer reports that its refractive index is 1.353 at 293 K. The measurement uncertainty is based on the standard deviation of 5 repeat measurements, where dilution of each sample was optimized. Importantly, no individual cluster can be monitored in the current system; therefore, colloidal sizes are monitored. Prior to the addition of the precursor reagents, solvents were prefiltered using a 0.2 μm filter to remove dust. The product from the methanol/$NaBH_4$ reaction was removed with centrifugation. In addition, DLS measurements were conducted on solutions containing dissolved ligands, $AuClPPh_3$ alone, $NaBH_4$ alone, and dissolved $NaBH_4$ and ligands together; these measurements exhibited null results, increasing the acceptance that the DLS distributions derived for reaction solutions correlate to $[Au_xL^6{}_y]^{z+}$ cluster formation only.

Synthesis Solution Preparation. The syntheses of PPh_3-protected Au clusters were conducted in several different mixtures; all performed in 20 mL of borosilicate crimp-sealed vials. For methanol mixtures, a 10.0 $\pm$ 0.1 mg (0.020 mmol) sample of $AuClPPh_3$ (Sigma Aldrich, 99.9%) was dissolved in 1:1 mixtures of methanol (Sigma Aldrich, HPLC grade) with either chloroform (Sigma Aldrich, ACS reagent) or diethyl ether (Sigma Aldrich, CHROMASOLV, 99.9%, inhibitor free) and mixed with a polytetrafluoroethylene (PTFE) coated, magnetic stirbar at 293 K for 30 min. Dry 3.5 $\pm$ 0.5 mg (0.093 mmol) $NaBH_4$ was added; this action established t_{react} = 0 min. The vial was sealed and allowed to stir for up to 5 days. An analogous procedure was used to prepare 1:1 ethanol (Sigma-Aldrich, 200 proof, HPLC/spectrophotometric grade)/chloroform mixtures except that measurements on synthesis solutions containing ethanol were conducted for up to 9 days. Prior to UV−vis measurements 1.0 mL samples were drawn from reaction vials and diluted 2:1 with either methanol or ethanol. Vial components and stir bars are not reused.

Colorimetric Assay. Prior to experimental startup, a 20 mL borosilicate crimp-seal vial of a test set is loaded with a magnetic PTFE coated stirbar, 15 mL of 1:1 alcohol/chloroform, 15.0 $\pm$ 0.2 mg (0.030 mmol) $AuClPPh_3$, and 37.5 $\pm$ 0.5 mg (0.090 mmol) L^3 ligand (L^3 = 1,3-bis(diphenylphosphino)propane). A second reagent solution containing 3$\times$ molar excess of L^3, is prepared by dissolving 0.090 mmol L^3 ligand into 15 mL of 1:1 alcohol/chloroform. The individual solutions are stirred for ~30 min. A colorimetric assay is initiated by adding 5.0 $\pm$ 0.5 mg

(0.13 mmol) crystalline $NaBH_4$ reducing agent to the crimp-seal vial containing the $AuClPPh_3$; this action establishes $t_{ca} = 0$ min, where t_{ca} is the digestion time of the colorimetric assay. Then quickly, 1.0 mL of test solution (from the Au_x:PPh_3 synthesis solution) and 1.0 mL of 3× molar excess L^3 solution is delivered into the crimp-seal vial, and the vial is sealed. The vial contents are stirred for 24 h in the dark. (Vial components and stirbars are not reused.) At $t_{ca} = 24$ h UV−vis spectroscopy measures the vial contents; the assay solution is expected to exhibit absorption bands at 420 and 585 nm. The individual weights, relative ratios, and percentages of $W^{8,9}_{585nm}$ and $\{Au_x: x \geq 10\}_{420\ nm}$ are measured. The limits for the integration were 400−450 nm and 530−650 nm for $W^{x\geq10}_{420nm}$ and $W^{8,9}_{585nm}$, respectively. The uncertainty (2σ) associated with the integrated areas evolves from the shift in the baseline in the UV−vis spectra and is estimated to be <10% for all samples.[65] Similar assays can be conducted successfully in alcohol/diethyl ether solvent mixtures. The alcohol chosen for each assay matches the alcohol of the test solution.

Acknowledgment. J.M.P. acknowledges the National Research Council for an associate fellowship.

Supporting Information Available: DLS distribution evolution after addition of assay reagent and discussion, expanded view of the cluster processing from $t_{react} = 0$ h to $t_{react} = 8$ h in the in assayed 1:1 methanol/diethyl ether solutions, UV−vis spectra of 1:1 ethanol/diethyl ether system, and UV−vis of increasing molar excess of PPh_3 in 1:1 methanol/diethyl ether solvent system at 72 h. This material is available free of charge *via* the Internet at http://pubs.acs.org.

REFERENCES AND NOTES

1. Bergeron, D. E.; Coskuner, O.; Hudgens, J. W.; Gonzalez, C. A. Ligand Exchange Reactions in the Formation of Diphosphine-Protected Gold Clusters. *J. Phys. Chem. C* **2008,** *112*, 12808–12814.
2. Bertino, M. F.; Sun, Z. M.; Zhang, R.; Wang, L. S. Facile Syntheses of Monodisperse Ultrasmall Au Clusters. *J. Phys. Chem. B* **2006,** *110*, 21416–21418.
3. Soejima, T.; Kimizuka, N. One-Pot Room-Temperature Synthesis of Single-Crystalline Gold Nanocorolla in Water. *J. Am. Chem. Soc.* **2009,** *131*, 14407–14412.
4. Schaaff, T. G.; Whetten, R. L. Controlled Etching of Au:SR Cluster Compounds. *J. Phys. Chem. B* **1999,** *103*, 9394–9396.
5. Qian, H. F.; Zhu, M. Z.; Lanni, E.; Zhu, Y.; Bier, M. E.; Jin, R. C. Conversion of Polydisperse Au Nanoparticles into Monodisperse Au-25 Nanorods and Nanospheres. *J. Phys. Chem. C* **2009,** *113*, 17599–17603.
6. Wilcoxon, J. P.; Provencio, P. Etching and Aging Effects in Nanosize Au Clusters Investigated Using High-Resolution Size-Exclusion Chromatography. *J. Phys. Chem. B* **2003,** *107*, 12949–12957.
7. Brown, L. O.; Hutchison, J. E. Convenient Preparation of Stable, Narrow-Dispersity, Gold Nanocrystals by Ligand Exchange Reactions. *J. Am. Chem. Soc.* **1997,** *119*, 12384–12385.
8. Tolman, C. A. Steric Effects of Phosphorus Ligands in Organometallic Chemistry and Homogeneous Catalysis. *Chem. Rev.* **1977,** *77*, 313–348.
9. van Leeuwen, P. W. N. M.; Kamer, P. C. J.; Reek, J. N. H.; Dierkes, P. Ligand Bite Angle Effects in Metal-Catalyzed C−C Bond Formation. *Chem. Rev.* **2000,** *100*, 2741–2769.
10. Wang, Z. X.; Ma, L. N. Gold Nanoparticle Probes. *Coord. Chem. Rev.* **2009,** *253*, 1607–1618.
11. Huang, X. H.; Neretina, S.; El-Sayed, M. A. Gold Nanorods: From Synthesis and Properties to Biological and Biomedical Applications. *Adv. Mater.* **2009,** *21*, 4880–4910.
12. Schmid, G.; Klein, N.; Korste, L.; Kreibig, U.; Schonauer, D. Large Transition-Metal Clusters. 6. Ligand-Exchange Reactions on $Au_{55}(PPh_3)_{12}Cl_6$—The Formation of a Water-Soluble Au_{55} Cluster. *Polyhedron* **1988,** *7*, 605–608.
13. Yang, Y. Y.; Chen, S. W. Surface Manipulation of the Electronic Energy of Subnanometer-Sized Gold Clusters: An Electrochemical and Spectroscopic Investigation. *Nano Lett.* **2003,** *3*, 75–79.
14. Caragheorgheopol, A.; Chechik, V. Mechanistic Aspects of Ligand Exchange in Au Nanoparticles. *Phys. Chem. Chem. Phys.* **2008,** *10*, 5029–5041.
15. Teo, B. K.; Shi, X. B.; Zhang, H. Pure Gold Cluster of 1-9-9-1-9-9-1 Layered Structure—A Novel 39-Metal-Atom Cluster $[(Ph3P)_{14}Au_{39}Cl_6]Cl_2$ with an Interstitial Gold Atom in a Hexagonal Antiprismatic Cage. *J. Am. Chem. Soc.* **1992,** *114*, 2743–2745.
16. Schmid, G. The Relevance of Shape and Size of Au-55 Clusters. *Chem. Soc. Rev.* **2008,** *37*, 1909–1930.
17. Schmid, G.; Pfeil, R.; Boese, R.; Bandermann, F.; Meyer, S.; Calis, G. H. M.; van der Velden, W. A. $Au_{55}[P(C_6H_5)_3]_{12}Cl_6$—A Gold Cluster of an Exceptional Size. *Chem. Ber* **1981,** *114*, 3634–3642.
18. van der Velden, J. W. A.; Bour, J. J.; Bosman, W. P.; Noordik, J. H. Synthesis and X-ray Crystal-Structure Determination of the Cationic Gold Cluster Compound $[Au_8(PPh_3)_7](NO_3)_2$. *J. Chem. Soc., Chem. Commun.* **1981,** 1218–1219.
19. McPartlin, M; Mason, R.; Malatest., L. Novel Cluster Complexes of Gold(0)−Gold(1). *J. Chem. Soc. D: Chem. Commun.* **1969,** 334.
20. Manassero, M.; Naldini, L.; Sansoni, M. New Class of Gold Cluster Compounds—Synthesis and X-ray Structure of the Octakis(triphenylphosphinegold) Dializarinsulphonate, $[Au_8(PPh_3)_8](Aliz)_2$. *J. Chem. Soc. D: Chem. Commun.* **1979,** 385–386.
21. Briant, C. E.; Hall, K. P.; Mingos, D. M. P. Synthesis and Structural Characterization of $[Au_6(PPh_3)_6](NO_3)_2\ 3CH_2Cl_2$—An Edge-Shared Bitetrahedral Gold Cluster. *J. Organomet. Chem.* **1983,** *254*, C18–C20.
22. Lo, C. T. F.; Karan, K.; Davis, B. R. Kinetic Studies of Reaction between Sodium Borohydride and Methanol, Water, and Their Mixtures. *Ind. Eng. Chem. Res.* **2007,** *46*, 5478–5484.
23. Liu, X.; Worden, J. G.; Huo, Q.; Brennan, J. R. Kinetic Study of Gold Nanoparticle Growth in Solution by Brust-Schiffrin Reaction. *J. Nanosci. Nanotechnol.* **2006,** *6*, 1054–1059.
24. Davis, R. E.; Gottbrath, J. A. Boron Hydrides. 5. Methanolysis of Sodium Borohydride. *J. Am. Chem. Soc.* **1962,** *84*, 895–898.
25. Qian, H. F.; Zhu, Y.; Jin, R. C. Size-Focusing Synthesis, Optical and Electrochemical Properties of Monodisperse $Au_{38}(SC_2H_4Ph)_{24}$ Nanoclusters. *ACS Nano* **2009,** *3*, 3795–3803.
26. Brown, H. C.; Mead, E. J.; Rao, B. C. S. A Study of Solvents for Sodium Borohydride and the Effect of Solvent and the Metal Ion on Borohydride Reductions. *J. Am. Chem. Soc.* **1955,** *77*, 6209–6213.
27. Finney, E. E.; Finke, R. G. Nanocluster Nucleation and Growth Kinetic and Mechanistic Studies: A Review Emphasizing Transition-Metal Nanoclusters. *J. Colloid Interface Sci.* **2008,** *317*, 351–374.
28. Pettibone, J. M.; Hudgens, J. W. Synthetic Approach for Tunable, Size-Selective Formation of Monodisperse, Diphosphine-Protected Gold Nanoclusters. *J. Phys. Chem. Lett.* **2010,** *1*, 2536–2540.
29. Shem, P. M.; Sardar, R.; Shumaker-Parry, J. S. One-Step Synthesis of Phosphine-Stabilized Gold Nanoparticles Using the Mild Reducing Agent 9-BBN. *Langmuir* **2009,** *25*, 13279–13283.
30. Alvarez, M. M.; Khoury, J. T.; Schaaff, T. G.; Shafigullin, M. N.; Vezmar, I.; Whetten, R. L. Optical Absorption Spectra of Nanocrystal Gold Molecules. *J. Phys. Chem. B* **1997,** *101*, 3706–3712.
31. Hudgens, J. W.; Pettibone, J. M.; Senftle, T. P.; Bratton, R. N.; Bergeron, D. E. Formation and Degradation of Diphosphine-Protected Gold Clusters. Unpublished experiments.
32. Hall, K. P.; Mingos, D. M. P. Homonuclear and Heteronuclear Cluster Compounds of Gold. *Prog. Inorg. Chem.* **1984,** *32*, 237–325.
33. Methanol/diethyl ether mixtures are suitable for DLS measurements because these mixtures do not exhibit the solvent domain light scattering exhibited by methanol/chloroform mixtures.

34. Filipe, V.; Hawe, A.; Jiskoot, W. Critical Evaluation of Nanoparticle Tracking Analysis (NTA) by Nanosight for the Measurement of Nanoparticles and Protein Aggregates. *Pharm. Res.* **2010,** *27*, 796–810.
35. Link, S.; El-Sayed, M. A. Size and Temperature Dependence of the Plasmon Absorption of Colloidal Gold Nanoparticles. *J. Phys. Chem. B* **1999,** *103*, 4212–4217.
36. van der Velden, J. W. A.; Bour, J. J.; Steggerda, J. J.; Beurskens, P. T.; Roseboom, M.; Noordik, J. H. Gold Clusters. Tetrakis[1,3-Bis(diphenylphosphino)propane]hexagold Dinitrate: Preparation, X-ray Analysis, and Au-197 Mossbauer and P-31[H-1] NMR-Spectra. *Inorg. Chem.* **1982,** *21*, 4321–4324.
37. In the same article, the authors prepared $[Au_6L^3{}_4]^{2+}$ by the reaction of $Au_4(PPh_3)_4I_2$ in a solution containing excess L^3.
38. Evans, D. G.; Mingos, D. M. P. Molecular-Orbital Analysis of the Bonding in Low Nuclearity Gold and Platinum Tertiary Phosphine Complexes and the Development of Isolobal Analogies for the $M(PR_3)$ Fragment. *J. Organomet. Chem.* **1983,** *232*, 171–191.
39. Bergeron, D. E.; Hudgens, J. W. Ligand Dissociation and Core Fission from Diphosphine-Protected Gold Clusters. *J. Phys. Chem. C* **2007,** *111*, 8195–8201.
40. Bos, W.; Bour, J. J.; Vandervelden, J. W. A.; Steggerda, J. J.; Casalnuovo, A. L.; Pignolet, L. H. Gold Clusters. Reactivity of $[Au_9(PPh_3)_8]^{3+}$ and $[Au_8(PPh_3)_7]^{2+}$ towards Isopropyl Isocyanide. *J. Organomet. Chem.* **1983,** *253*, C64–C66.
41. van der Velden, J. W. A.; Bour, J. J.; Bosman, W. P.; Noordik, J. H. Reactions of Cationic Gold Clusters with Lewis-Bases. Preparation and X-ray Structure Investigation of $[Au_8(PPh_3)_7](NO_3)_2 \cdot 2CH_2Cl_2$ and $Au_6(PPh_3)_4[Co(CO)_4]_2$. *Inorg. Chem.* **1983,** *22*, 1913–1918.
42. van der Linden, J. G. M.; Paulissen, M. L. H.; Schmitz, J. E. J. Electrochemical Reduction of the Gold Cluster $Au_9(PPh_3)_8{}^{3+}$. Evidence for an ErErCr Mechanism. Formation of the Paramagnetic Gold Cluster $Au_9(PPh_3)_8{}^{2+}$. *J. Am. Chem. Soc.* **1983,** *105*, 1903–1907.
43. van der Velden, J. W. A.; Beurskens, P. T.; Bour, J. J.; Bosman, W. P.; Noordik, J. H.; Kolenbrander, M.; Buskes, J. A. K. M. Intermediates in the Formation of Gold Clusters. Preparation and X-ray Analysis of $[Au_7(PPh_3)_7]^+$ and Synthesis and Characterization of $[Au_8(PPh_3)_6I]PF_6$. *Inorg. Chem.* **1984,** *23*, 146–151.
44. Mingos, D. M. P. Structure and Bonding in Cluster Compounds of Gold. *Polyhedron* **1984,** *3*, 1289–1297.
45. King, R. B. Metal Cluster Topology. 2. Gold Clusters. *Inorg. Chim. Acta* **1986,** *116*, 109–117.
46. Shichibu, Y.; Negishi, Y.; Tsukuda, T.; Teranishi, T. Large-Scale Synthesis of Thiolated Au_{25} Clusters *via* Ligand Exchange Reactions of Phosphine-Stabilized Au_{11} Clusters. *J. Am. Chem. Soc.* **2005,** *127*, 13464–13465.
47. Haberlen, O. D.; Rosch, N. Effect of Phosphine Substituents in Gold(1) Complexes: A Theoretical Study of $MeAuPR_3$, R = H, Me, Ph. *J. Phys. Chem.* **1993,** *97*, 4970–4973.
48. Schwerdtfeger, P.; Hermann, H. L.; Schmidbaur, H. Stability of the Gold(I)−Phosphine Bond. A Comparison with Other Group 11 Elements. *Inorg. Chem.* **2003,** *42*, 1334–1342.
49. Golightly, J. S.; Gao, L.; Castleman, A. W.; Bergeron, D. E.; Hudgens, J. W.; Magyar, R. J.; Gonzalez, C. A. Impact of Swapping Ethyl for Phenyl Groups on Diphosphine-Protected Undecagold. *J. Phys. Chem. C* **2007,** *111*, 14625–14627.
50. Shafai, G.; Hong, S. Y.; Bertino, M.; Rahman, T. S. Effect of Ligands on the Geometric and Electronic Structure of Au_{13} Clusters. *J. Phys. Chem. C* **2009,** *113*, 12072–12078.
51. Gorin, D. J.; Toste, F. D. Relativistic Effects in Homogeneous Gold Catalysis. *Nature* **2007,** *446*, 395–403.
52. Leadbeater, N. E.; Marco, M. Preparation of Polymer-Supported Ligands and Metal Complexes for Use in Catalysis. *Chem. Rev.* **2002,** *102*, 3217–3273.
53. The Au atoms added and removed though reaction 3 and reaction 4 will be ligated. The definition of a ligand is not confined only to the phosphorous species, but includes $Au\text{-}PPh_3$, $Ph_3P\text{-}Au\text{-}PPh_3$, $Au\text{-}Au\text{-}PPh_3$, and similar mono- and digold species with other diphosphine ligands, L^n.
54. Jin, R.; Qian, H.; Wu, Z.; Zhu, Y.; Zhu, M.; Mohanty, A.; Garg, N. Size Focusing: A Methodology for Synthesizing Atomically Precise Gold Nanoclusters. *J. Phys. Chem. Lett.* **2010,** 2903–2910.
55. Brown, L. O.; Hutchison, J. E. Controlled Growth of Gold Nanoparticles during Ligand Exchange. *J. Am. Chem. Soc.* **1999,** *121*, 882–883.
56. IUPAC. *The Gold Book: Compendium of Chemical Terminology* , 2nd ed.; Blackwell Scientific Publications: Oxford, 1997. http://Goldbook.Iupac.Org (accessed May 2010).
57. Watzky, M. A.; Finke, R. G. Transition Metal Nanocluster Formation Kinetic and Mechanistic Studies. A New Mechanism When Hydrogen Is the Reductant: Slow, Continuous Nucleation and Fast Autocatalytic Surface Growth. *J. Am. Chem. Soc.* **1997,** *119*, 10382–10400.
58. Finney, E. E.; Finke, R. G. Fitting and Interpreting Transition-Metal Nanocluster Formation and Other Sigmoidal-Appearing Kinetic Data: A More Thorough Testing of Dispersive Kinetic *vs* Chemical-Mechanism-Based Equations and Treatments for 4-Step Type Kinetic Data. *Chem. Mater.* **2009,** *21*, 4468–4479.
59. Watzky, M. A.; Finney, E. E.; Finke, R. G. Transition-Metal Nanocluster Size *vs* Formation Time and the Catalytically Effective Nucleus Number: A Mechanism-Based Treatment. *J. Am. Chem. Soc.* **2008,** *130*, 11959–11969.
60. Mosseri, S.; Henglein, A.; Janata, E. Reduction of $Au(CN)_2$ in Aqueous-Solution: Formation of Nonmetallic Clusters and Colloidal Gold. *J. Phys. Chem.* **1989,** *93*, 6791–6795.
61. Henglein, A.; Meisel, D. Radiolytic Control of the Size of Colloidal Gold Nanoparticles. *Langmuir* **1998,** *14*, 7392–7396.
62. Majimel, J.; Bacinello, D.; Durand, E.; Vallee, F.; Treguer-Delapierre, M. Synthesis of Hybrid Gold−Gold Sulfide Colloidal Particles. *Langmuir* **2008,** *24*, 4289–4294.
63. Certain commercial materials and equipment are identified in this paper in order to adequately specify the experimental procedure. Such identification neither implies recommendation or endorsement by the National Institute of Standards and Technology nor does it imply that the material or equipment identified is the best available for the purpose.
64. *CRC Handbook of Chemistry and Physics*, 91st ed.; CRC Press: Boca Raton, FL, 2010—2011. http://www.hbcpnetbase.com (accessed May 10, 2010).
65. The molar absorbtivity, ε, of each product formed through L^3 addition was not measured, but determination of ε for each species representing the 420 and 585 nm absorption bands would allow for accurate concentration measurements.